

More precise edge detections

Hao Shu^{†*}

[†] Shenzhen University, Shenzhen, China.

Abstract—Image Edge detection (ED) is a base task in computer vision. While the performance of the ED algorithm has been improved greatly by introducing CNN-based models, current models still suffer from unsatisfactory precision rates especially when only a low error toleration distance is allowed. Therefore, model architecture for more precise predictions still needs an investigation. On the other hand, the unavoidable noise training data provided by humans would lead to unsatisfactory model predictions even when inputs are edge maps themselves, which also needs a solution. In this paper, more precise ED models are presented with cascaded skipping density blocks (CSDB). Our models obtain state-of-the-art(SOTA) predictions in several datasets, especially in average precision rate (AP), over a high-standard benchmark, which is confirmed by extensive experiments. Also, a novel modification on data augmentation for training is employed, which allows noiseless data to be employed in model training for the first time, and thus further improves the model performance. The relative Python codes can be found on <https://github.com/Hao-B-Shu/SDPED>.

I. INTRODUCTION

Being studied for decades, image edge detection (ED) is one of the foundation tasks in computer versions with a wide application in high-level tasks such as object detection[1] and image segmentation[2]. Early works of ED tasks such as Sobel operator[3] and Canny algorithm[4] employed gradients as the distinguished feature, and later, more statistical methods were presented[5, 6]. Recent years, as machine learning plays an irreplaceable role in nearly all computer vision tasks, substantial learning-based algorithms were proposed[7–12], and so far the conventional neural network(CNN) models achieve in state-of-the-art (SOTA)[12–23].

ED task aims to find edges in an image, usually including pixels with significant changes compared with their neighbors. However, textural areas could also contain rapidly-changed pixels, although they are not considered to be edges in most cases. Since it is difficult to define texture strictly, classical algorithms such as Canny[4], despite being efficient, usually could not provide satisfactory results, as they cannot adjust themselves in variable data. Therefore, learning-based models such as CNN ones gradually become the mainstream. In the last decade, great progress has demonstrated the ability and potential of CNN-based ED models. The F -score of SOTA models such as HED[15], RCF[16], RIND[24], BDCN[25], Dexi[23], and even lightweight ones such as TEED[26] can close to or exceed the one provided by humans in the standard evaluation procedure.

Nevertheless, some unignorable issues also occurred, and the following two are considered in this paper.

(i) Current models can obtain high scores only when a large range of error toleration is applied. For example, the error

toleration radius is usually set to be about 4.3 pixels in dataset BSDS500[6], 11.1 pixels in dataset BIPED[27], and even 16.3 pixels in dataset MDBD[28]. When the evaluation standard becomes stricter, their scores decrease significantly, especially in average precision rate (AP). Hence, more precise models, especially over a high standard, need to be designed.

(ii) Current models always produce unsatisfactory edges on noiseless data, namely when the inputs are edge maps themselves, as shown in Fig1. Indeed, the predictions on noiseless data are usually similar to the predictions on noise data, namely the ordinary images, which is unacceptable. Since the edge maps have deleted all textural regions, a model is expected to produce better outcomes on them. Such an issue needs a solution¹.

In this paper, we propose novel ED models with cascaded skipping density blocks (CSDB). Density blocks (DB) have been employed in other computer vision tasks such as image super-resolution(SR)[29] and have shown their ability. However, such structures do not perform well when directly applied to ED tasks. Therefore, we modify them by proposing CSDB which is more suitable for ED tasks, and design novel ED models based on it. On the other hand, to improve the performance of models on noiseless data, we make efforts on data augmentations. Usual data augmentations in ED tasks do not include noiseless data, and consequently, models never learned from noiseless data, which could be the main reason that previous models provide similar outcomes no matter whether the inputs are noise images with textures or noiseless edge maps without any texture. In fact, accessing noiseless data in ED tasks seems impossible, for human annotations are the only way to provide groundtruths. However, we employ a trick in the data augmentation, which allows noiseless data for model training. The main contributions of this paper include:

(1) Precise models for ED tasks are proposed, providing the most precise outputs so far and obtaining SOTA results. The presenting models, named skipping density precise edge detection and denoted by SDPED for short, employ very deep structures with CSDB, which have not been considered in ED yet. On the other hand, the presenting models do not need supervision in different scales, demonstrating the unnecessary of multiply-scales supervising, while multiply-scales supervising was widely believed as necessary in previous studies.

(2) A novel modification in data augmentation is proposed, allowing ED models to employ noiseless data for training, and thus provide more satisfactory results on noiseless

¹We consider the ordinary images to be ones generated from the edge maps by adding noises (such as textures). Therefore, in this paper, by noiseless data, we mean the edge maps themselves, while by noise data, we mean the ordinary images. In such a context, models are expected to provide better results on noiseless data than on noise data.

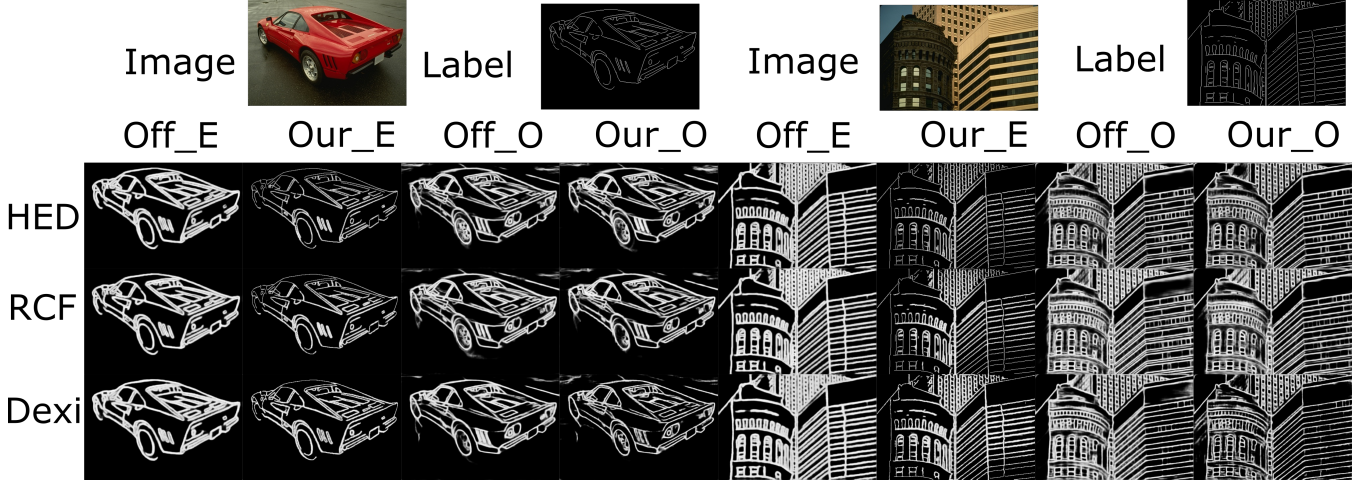


Fig. 1 Results of three previous models implemented on dataset BRIND, where, *Off_E* represents that the model is retrained following the off data augmentation and predicts on the edge map, *Our_E* represents that the model is retrained following our data augmentation provided in Section III B (or Section IV A 2)) and predicts on the edge map, *Off_O* represents that the model is retrained following the off data augmentation and predicts on the ordinary image, and *Our_O* represents that the model is retrained following our data augmentation method, which allows more precise (crisper) predictions on edge maps themselves and might also improve the predictions on ordinary images.

data. So far, it could be the only solution for the issues in aforementioned (ii) and Fig1.

(3) Extensive experiments are launched to support the validity of findings.

II. PREVIOUS WORK

In this section, some related previous works including datasets and pre-processing, CNN-based ED models and loss functions, as well as result evaluations are reviewed.

A. Datasets, label refinements, and data augmentations

Early datasets for ED tasks were directly taken from segmentation tasks. Among them, the most employed one was the BSDS300 which later extended to BSDS500[30]. Dataset BSDS500 contains 500 RGB images with labels provided by multiple annotators and was widely employed in boundary detection as well as segmentation tasks. Another well-known dataset is the NYUD/NYUD2[31]. NYUD2 dataset includes hundreds of thousands RGBD images comprised of video sequences from a variety of indoor scenes, among which 1449 images are labeled with segmentation categories. Other common used datasets include PASCAL VOC[32], Microsoft COCO[33], SceneParse150[34], and Cityscape[35].

However, most of the datasets are not ordinarily for the ED task, and thus the labels might not be suitable. In recent years, with the growth of attention in the ED community, several datasets specific to ED have been proposed. In 2016, dataset MDBD[28] with 100 scenes and 10 sampled frames in each was provided, ordinarily for boundary detection tasks and can also be employed in ED tasks, which contains 100 high-resolution (1280×720) images labeled by multiple annotators. In 2020, dataset BIPED[27] was presented for edge detection tasks particularly, which contains 250 high-resolution (1280×720) RGB images with labeled edges, and later modified to BIPED2. In 2021, dataset BRIND[24] was proposed

by directly re-annotating on BSDS500, which classified edges into four types, namely reflectance edge, illumination edge, normal edge, and depth edge. And in 2023, dataset UDED[26] was proposed by picking several high-quality images from several datasets. The images are labeled carefully but it only contains 29 images.

The most serious problem in all datasets is that the annotation can never be noiseless. Human annotations are unavoidable to be employed in ED datasets. However, as long as edges are labeled by humans, it can never be accurate and could always vary from one to another. Therefore, several works focusing on improving labels marked by humans or improving model performance under noisy labels were presented[36, 37].

No matter which datasets are employed in ED tasks, a consensus is that data augmentations are necessary. Data augmentations usually include image rotations, flips, crops, resizing, and gamma transformations. However, the augmentation procedures are different from paper to paper. In HED[15], the images are rotated by 16 different angles with flips, and the largest rectangles are cropped, obtaining 32 images from each one. In RIND[24], Only 4 angle rotations are implemented with flips and without crops, obtaining 8 images from each. While in Dexi[23], 16 rotations with flips, crops, and 3 gamma transformations are applied, obtaining 288 images from each. Seldom studies were conducted to demonstrate the validity of mass augmentation, but obviously, more augmentations result in higher consumption of model training.

B. CNN-based ED models and loss functions

CNN-based methods are the mainstream in ED tasks currently. HED[15] outputs results in multi-scales and multi-levels and then fuses them, while the loss is calculated as the average of all outputs in supervising. RCF[16] not only employs multi-scale outputs as in HED but also fuses different features in different layers to obtain side outputs. In BDCN[25], different

supervisions are applied in different layers. In PiDiNet[20], pixel difference convolutions are implemented and the model is also supervised via outputs provided by different scales. RIND[24] separately predicts four kinds of edges with three stages and Dexi[23] adopts extremely dense skip connections.

Most of the CNN-based models cannot output crisp edges without post-processing such as non-maximal suppression (NMS). This might be caused by the max-pool operation in down-samples and the employment of weight binary cross entropy (WBCE) as the loss function. There are studies on obtaining thinner edges, such as combining features on the larger scale when up-sample[38] and employing dice loss[39]. Recent work showed that employing tracing-loss[21] as the loss function might be a solution and it has been implemented in several models such as TEED[26]. Although these methods have provided extra options, their employment might result in a cost in other ways.

C. Prediction evaluations

The standard procedure for evaluating ED models is calculating the optimal dataset scale (ODS), optimal image scale (OIS), and average precision rate (AP), based on the F_β -score calculated as $\frac{(1+\beta^2) \times \text{precision} \times \text{recall}}{\beta^2 \times \text{precision} + \text{recall}}$, where *precision* represents the precision rate calculated by $\frac{TP}{TP+FP}$, *recall* represents the recall rate calculated by $\frac{TP}{TP+FN}$, and β is a coefficient representing the trade-off between precision rate and recall rate, typically set to be 1. Here, *TP* is the number of edge pixels (in the groundtruth) that are predicted to be edge pixels by the model, *FP* is the number of non-edge pixels (in the groundtruth) that are predicted to be edge pixels by the model, and *FN* is the number of edge pixels (in the groundtruth) that are predicted to be non-edge pixels by the model.

Most models employ the evaluation algorithm provided in [7] to assess results. In the algorithm, there is a hyperparameter called *maxDist* representing the maximal distance of error toleration². It is worth noting that seldom studies are conducted on which error toleration distance is the most reasonable one, which results in inconsistent employment. For example, the error toleration distance was set to be 0.0075 in BSDS500 dataset[30], namely about 4.3 pixels, 0.0075 in BIPED dataset[23], becomes 11.1 pixels since the resolution of the images is higher, while 0.011 in MDBD dataset[28], about 16.3 pixels. Certainly, decreasing the error toleration distance would allow a stricter standard.

III. METHODOLOGY

A. The SDPED model

The structure of the presenting SDPED model is displayed in Fig2 with illustrations in Fig3, Fig4. It employs CSDB in the main path, providing multiple outputs which then be fused by the fusing block. DB is typical in some other computer vision tasks such as SR[29, 40], and its validity has been

demonstrated by experiments, namely it can be applied to process textures in an image. As the main difficulty in both the SR task and ED task is dealing with texture regions, it is worth trying to utilize similar structures in the latter. However, for applying to the ED task, modifications are needed, and we replace DB with CSDB which could be more suitable for such tasks. Moreover, in contrast to previous models usually fused multiple outputs by a single 1×1 convention layer, we find that a more complicated structure could provide better performance. Here, we employ three convention layers in the fusing block including one 3×3 convention layer.

The model employs weight binary cross entropy loss L_{WBCE} as the loss function in training, defined as:

$$L_{WBCE}(\hat{Y}, Y) = -\alpha \sum_{\hat{y}_i \in Y^+} \log(\hat{y}_i) - \lambda(1-\alpha) \sum_{\hat{y}_i \in Y^-} \log(1-\hat{y}_i) \quad (1)$$

where Y^+ is the set of positive samples, namely edge pixels in the groundtruth, Y^- is the set of negative samples, namely non-edge pixels in the groundtruth, α is the proportion of the number of negative samples, namely $\alpha = \frac{|Y^-|}{|Y|}$.

B. Improving the performance on noiseless data

Previous models (or in fact data augmentation methods) always provide unsatisfactory results on noiseless data. As edge maps (noiseless data) do provide significantly higher-quality information on edges compared with images themselves, the predictions on them are expected to be more precise and beautiful than on the ordinary images (noise data). However, under previous settings, the results on noiseless data are usually similar to the results on noise data, as displayed in Fig1.

The obvious reason for such an issue is that previous models are trained on datasets labeled by humans, which are unavoidably noisy. Missing, error, and over-annotation in human labels can be serious in ED tasks. Certainly, the solution of it is adding noiseless data into training sets. Unfortunately, so far, human labels could be the only way to provide groundtruths in practice and thus it seems impossible to obtain noiseless data.

However, what if we add labels to the training set directly? Labels, no matter how they are obtained, could be considered as noiseless data since they are the groundtruths being employed. By such an observation, noiseless data can be obtained and employed as a part of the dataset (with the labels being themselves). This could be the only way to access noiseless data, currently. With such a modification on data augmentation, models could provide more satisfactory predictions on noiseless data as exhibited in Fig1.

C. Suitable error toleration distance

To evaluate models on a given dataset, the most employed algorithm is the one provided in [7] to calculate ODS, OIS, and AP, under a range of error toleration distance. However, the error toleration distance is set differently among different researchers, from about 4.3 pixels in BRIND[30],

²It is interpreted as the ratio of diagonal distance. For example, in dataset BSDS500 with image resolution 321×481 , the toleration distance is calculated as $\sqrt{481^2 + 321^2} \times \text{maxDist} \approx 4.3 \text{ Pixels}$, if $\text{maxDist} = 0.0075$

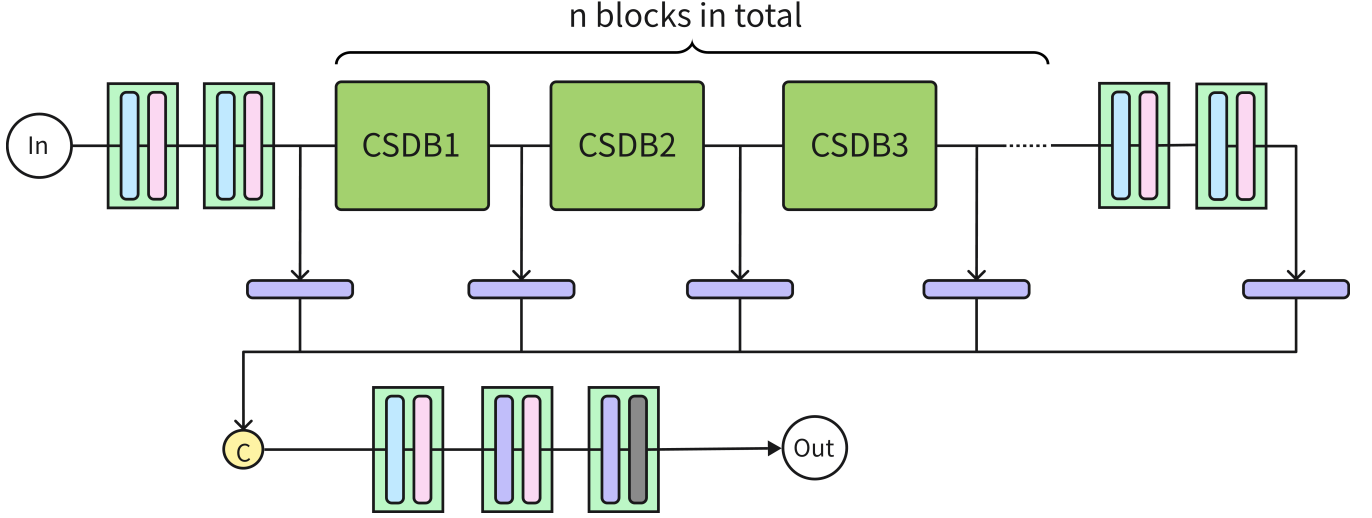


Fig. 2 The SDPED model: **Top path** is the main path of the model. Typically, the first 2 convention layers output 32 and 64 features, while the number of input and output features in the last two convention layers are all 64. $n + 2$ layers, including the feature extractor block, each CSDB, and the last block, would provide middle results, where each would be fused into 21 features. All middle results are concatenated to obtain $21 \times (n + 2)$ features for the final fusing layer (the button path). **Button path** is the fusing block, where the $21 \times (n + 2)$ features from the main path goes through one 3×3 convention block and then two 1×1 convention blocks. The numbers of the output features of such layers are 256, 512, and 1, respectively.

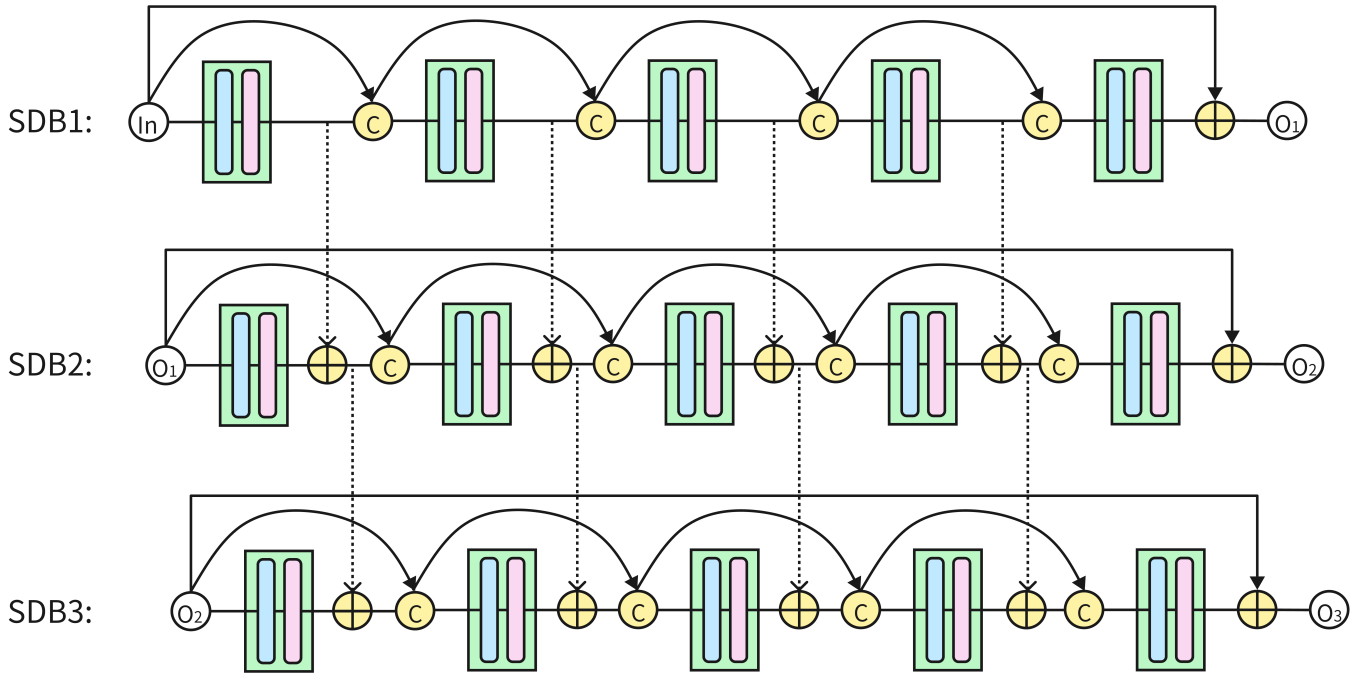


Fig. 3 Cascading skipping dense block (CSDB): Typically, there are 5 conversion layers in a single SDB block. The number of input features is set to 64, and each of the first 4 layers outputs 32 features. Therefore, the number of input features becomes 96, 128, 160, and 192, in the second, third, fourth, and final layers, respectively. The final layer outputs 64 features. Several (typically 3) SDB are cascaded with skipping connections to form a CSDB.

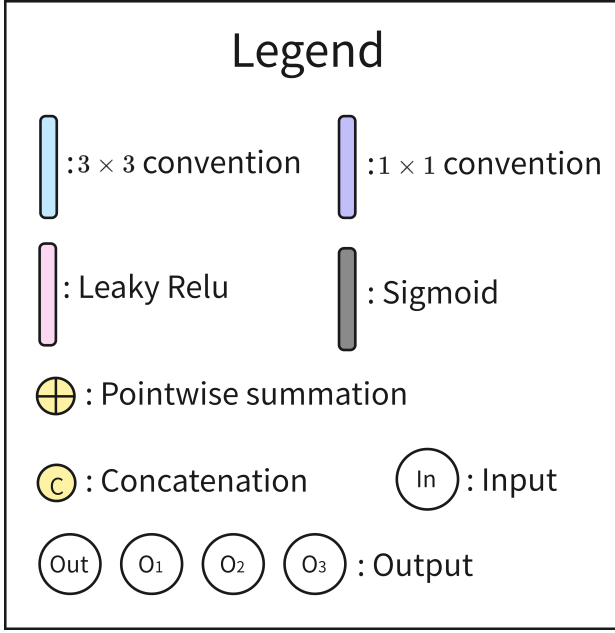


Fig. 4 Legend

11.1 pixels in BIPED[23], and even 16.3 pixels in MDBD dataset[28]. Most authors did not modify the default setting in the evaluation algorithm in which the error toleration distance is set to be a fixed ratio of the diagonal distance, resulting in different benchmarks even when the coefficient is set to be the same³. Employing the ratio of diagonal distance as the error toleration radius seems not reasonable enough, since the standard will be relaxed when the resolution of the image is increased. For example, in the BSDS500 dataset with image resolution 321×481 , nearly 4.3 pixels errors are allowed by fixing ratio 0.0075, while the toleration range would be twice to about 8.6 pixels if four predictions are evaluated together by simply concatenating to a 642×962 image. Consequently, the evaluation score can be much higher by concatenating more predictions, even though ordinary data is never changed. To allow the evaluation independent of the resolution of the images, we suggest that the error toleration distance be set to be an exact length of pixels instead of a ratio of the diagonal distance.

On the other hand, how many pixels of error toleration is suitable in ED tasks is seldom discussed. In this paper, we consider that models should be evaluated on a low error toleration distance since a model obtains a low score on a tight error toleration benchmark while obtaining a high score on a loose one represents that error pixels do make unreasonable contributions⁴. On the other hand, certainly,

³The error toleration distance in pixels could be different under the same ratio of the diagonal distance. For example, in BRIND consisting of images with resolution 321×481 , 0.0075 error toleration distance ratio represents about 4.3 pixels, while in BIPED consisting of images with resolution 720×1280 , it represents 11.1 pixels.

⁴For example, the prediction with a pixel missing on edge should have a higher score than the one with a pixel missing on edge and in addition a pixel error on non-edge. However, a loose error toleration distance has a higher probability of allowing the latter to have a higher score since it might predict an edge pixel incorrectly but could in the error toleration distance.

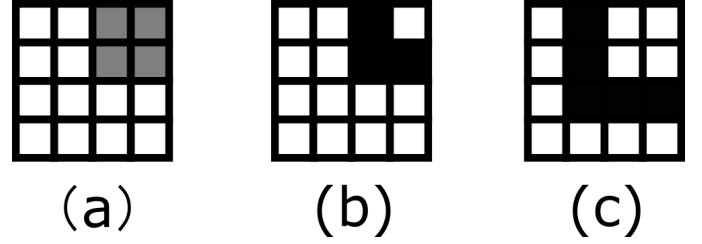


Fig. 5 For a local image of style as (a), edges are usually labeled as style (b) or (c) in current datasets, both reasonable for 1-pixel wide edges, wherein (b) and (c), black squares represent edge pixels. Here, no-corner edge pixels might have a 1-pixel deviation in horizontal or vertical while corner edge pixels might have a 1-pixel deviation in the diagonal direction.

models are expected to be as precise as possible, which also indicates the suitability of a strict error toleration distance.

However, notice that edge annotations in current datasets labeled by humans usually have a 1-pixel deviation since humans tend to mark edges with 1-pixel wide but edges can have 2-pixels wide in general, as shown in Fig5. If all annotations are in the same type, then no error toleration represents the tightest standard. But in practice, human labels could mix both types, resulting in usually at most a 1-pixel deviation. Therefore, 1-pixel error toleration could be considered as the tightest threshold on current datasets with labels provided by humans, while more than 1-pixel error toleration could improve the contributions of errors. Hence, we suggest error toleration threshold be 1 pixel for a strict standard in evaluations.

IV. EXPERIMENT

A. Settings and benchmarks

1) *Datasets*: Experiments are implemented on dataset BRIND[24], dataset UDED[26], dataset MDBD[28], and dataset BIPED[27]. For BRIND, we union all labels to one binary map for each image⁵. For MDBD, we employ annotation 3 as the labels⁶. For UDED and BIPED, labels are unique. Also note that among all the four datasets, the quality of UDED is the highest, while BRIND contains the richest images.

2) *Data augmentations*: Training images are split halved until the height and width are both lower than 640 pixels, then they are rotated by 0° , 90° , 180° , 270° with flips, obtaining 8 augmentation images for each image after being split. In addition, labels are added into the training set as data with groundtruths set to be themselves to improve the performance on noiseless data. In training, the images are randomly cropped to 320×320 , and data is refreshed every 5 epochs. Also for convenience, we focus the two images in UDED whose width is lower than 320 pixels to be the test images to avoid resizing in training.

⁵We simply union the different groundtruths as a binary map for each image in the paper, namely, a pixel is considered as an edge pixel if it is an edge pixel in any groundtruths.

⁶It is not because annotation 3 is special, but is randomly chosen. We have tried employing the union of some or all of the 6 labels, but found that the qualities are not good enough.

3) *Training notes*: The optimizer of all models is set to be Adam with 10^{-8} weight decay. The learning rate begins by 10^{-4} and is divided by 10 after every 50 epochs. Batch size is set to be 8 and $\lambda = 1.1$ in equation (1).

4) *Evaluation and comparison benchmarks*: Predictions are implemented on test images⁷ of full resolutions and evaluated by the standard algorithm[7], with the most precise error toleration distance, namely 1 pixel in diagonal (or about 1.42 to 1.99 pixels in horizontal and vertical) as suggested in the above section. The corresponding error toleration distance can be taken as 0.003 for BRIND, and 0.001 for MDBD and BIPED, respectively. For UDED consisting of images with different resolutions, it is set to be 0.004 so that the smallest image with resolution 250×361 is with 1-pixel error toleration.

We compare the presenting models with HED[15], RCF[16], RIND[24], BDCN[25], Dexi[23]. All previous models employed in comparisons are retained by loss functions following their default settings. All models are trained under the same setting including the same data, the same optimizer, the same normalization, and the same save procedure of the predictions, for fairness. Epochs 100 for BRIND, 150 for UDED, 100 for MDBD, and 75 for BIPED are employed for all models. The SDPED models can be set with multiple lengths, namely with different numbers of CSDB blocks⁸, and typically SDPED_7 is employed for comparisons.

As pointed out in [41], most of the models obtaining SOTA results in a dataset are at the cost of generalizing ability and when the dataset set is changed, the performance becomes significantly degraded⁹. Therefore, to provide an extensive and reliable comparison, we implement experiments on several datasets, each with multiple partitions. Note that we employ '*Dataset- P_k -a-b-Ec*' to index the partition of the dataset and it is read as '*The result corresponds to Dataset on the k -th partition, where the training set consists of a images, the test set consists of b images, and Epoch c is employed*'. For example, '*BRIND- P_1 -250-250-E100*' represents that the result is on the dataset BRIND, and is on the 1-st partition, where the training set consists of 250 images, the test set consists of 250 images, and Epoch 100 is employed.

B. Experiment results

The evaluation results on BRIND, UDED, MDBD, and BIPED2 are shown in TableI, TableII, TableIII, and TableIV, respectively, and some predicted images are displayed in Fig6. Our models obtain SOTA results compared with previous ones. On BRIND, the score of our model improves about 2.7% on ODS, 3.1% on OIS, and 6.9% on AP on average. On UDED, the score of our model improves about 5.2% on ODS, 4.4% on OIS, and 2.4% on AP on average. On MDBD, the score of our model improves about 4.8%/2.5% on ODS, 4.8%/2.9% on OIS, and 22.5%/14.7% on AP, regarding error toleration 0.001/0.003 (1.5 pixel / 4.4 pixels in horizontal and vertical). On BIPED2, our model significantly outperforms previous

ones in AP (improves about 11.8% on average), while it obtains comparable results in ODS and OIS (different less than 0.3% on average, no matter it or the previous ones obtain the best scores).

C. Ablation studies

We provide ablation studies on BRIND and UDED to verify the effectiveness of the skipping dense structure and the multiple-layer fusing block. TableV demonstrates they do provide contributions.

V. DISCUSSION AND LIMITATION

A. Why SDPED effective?

The reasons for the improvement of the SDPED models, especially on AP, could be explained as follows. (1) most previous models employ down-sample methods such as max-pool in their structure to obtain multiple scale outputs. Such operations usually result in the loss of information in the ordinary image. As an example, when employing the 2×2 max-pool operation, information of 4 pixels is mixed and can not be distinguished again. Therefore, such operations could lead to the reduction of the precise rate, since the uncertainty is increased. On the other hand, in SDPED models, no down-sample operations are included, and thus no information is lost attributed to such an issue¹⁰. (2) The performance of ED models depends on the ability of them to deal with the textures. In such a context, simple conventional operations might not be sufficient as has been shown in most computer version tasks. The backbone of SDPED models has demonstrated its ability to deal with textures in SR tasks. Since the difficulty in SR tasks and in ED tasks are both finding textural areas, similar architectures might provide benefits¹¹. (3) The greatest difficulty in ED tasks is whether a pixel belonging to edges depends on its response under certain criteria, typically gradient but usually more complex. The main problem is that textural areas can also respond significantly to such criteria. To distinguish the edges from the textures, one needs to find those areas with 'the most response' areas. In SDPED, the CSDB is designed under such an observation. If a pixel has a high response only on one of the layers(SDB) in a CSDB but low on others, it will provide a low final response since the skipping connections. Hence, the 'most response' pixels are preserved while others are suppressed¹².

¹⁰Down-sample operations are widely believed as necessary in previous ED works, since multiple-scale information can be important in such tasks, which were demonstrated in traditional models[9]. This might be the reason that most previous CNN-based models inherited such operations. However, in deep CNN models, the wide receptive field can cover the information from multi-scales, and thus down-sample operations can be redundant. Therefore, as it results in the loss of information and increasing uncertainty, Removing them might be better.

¹¹In SR tasks, one needs to find the textural areas and add textures, while in ED tasks, one needs to find the textural areas and deleted textures. Therefore, a backbone performing well in SR tasks implies that it performs well in finding texture areas, and thus might be significant in ED tasks.

¹²A CSDB might be viewed as making the decision by averaging the intensity of all SDB response, and thus pixels considered as edge ones by all SDB have the strongest response while those only considered as edge pixels by fewer SDB are suppressed.

⁷All tests do not include noiseless data unless special pointed out.

⁸Here SDPED_n represents that the model has n CSDB blocks.

⁹This issue can occur even when only changing the partitions (into the training set and the test set) of the same dataset

TABLE I

Results on BRIND with error toleration 0.003 (1 pixel on diagonal), where the best results are marked as **blue**, while the second best ones are marked as **red**. In all the three experiments and all the three benchmarks, our model (SDPED_7) obtains the best results. The improvements compared with the second-best ones (on each partition and benchmark, no matter whether they are obtained by the same previous model or not) are also listed. On average, the score of our model improves about 2.7% on ODS, 3.1% on OIS, and 6.9% on AP, respectively.

Partitions	BRIND- P_1 -250-250-E100			BRIND- P_2 -300-200-E100			BRIND- P_3 -400-100-E100		
Benchmarks	ODS	OIS	AP	ODS	OIS	AP	ODS	OIS	AP
HED (2015)	0.639	0.651	0.575	0.657	0.669	0.597	0.663	0.675	0.605
RCF (2017)	0.643	0.653	0.573	0.663	0.672	0.598	0.665	0.674	0.603
RIND (2021)	0.624	0.634	0.509	0.651	0.661	0.610	0.649	0.662	0.590
BDCN (2022)	0.639	0.652	0.567	0.645	0.659	0.576	0.662	0.673	0.587
Dexi (2023)	0.639	0.648	0.548	0.652	0.663	0.572	0.663	0.674	0.585
SDPED_7 (Ours)	0.660	0.672	0.613	0.677	0.693	0.643	0.687	0.698	0.658
Improve	+2.6%	+2.9%	+6.6%	+2.1%	+3.1%	+5.4%	+3.3%	+3.4%	+8.8%
The results of the SDPED model with lengths 5 and 3 are listed below									
SDPED_5 (Ours)	0.660	0.672	0.616	0.676	0.692	0.645	0.683	0.693	0.649
SDPED_3 (Ours)	0.654	0.668	0.617	0.674	0.687	0.647	0.684	0.695	0.658

TABLE II

Results on UDED with error toleration 0.004 (1 pixel on the diagonal for the least resolution image), where the best results are marked as **blue**, while the second best ones are marked as **red**. In all the three experiments and all the three benchmarks, our model obtains the best results. The improvements compared with the second-best ones are also listed. On average, the score of our model (SDPED_7) improves about 5.2% on ODS, 4.4% on OIS, and 2.4% on AP, respectively. Also note that some results(P_1 and P_2) of RIND are far from satisfactory while some (P_3) are better. Such an issue occurs frequently and demonstrates that RIND might be not stable enough. Indeed, we retrain RIND on P_2 three times and all results are with very low AP, while retrain it on P_2 three times in which two are with very low AP. We retrain RIND on P_3 only once.

Partitions	UDED- P_1 -18-11-E150			UDED- P_2 -20-9-E150			UDED- P_3 -13-14-E150		
Benchmarks	ODS	OIS	AP	ODS	OIS	AP	ODS	OIS	AP
HED (2015)	0.714	0.732	0.687	0.709	0.733	0.673	0.639	0.675	0.590
RCF (2017)	0.737	0.775	0.713	0.746	0.763	0.724	0.637	0.703	0.609
RIND (2021)	0.416	0.425	0.071	0.375	0.381	0.046	0.716	0.747	0.678
BDCN (2022)	0.767	0.787	0.763	0.772	0.803	0.757	0.689	0.762	0.686
Dexi (2023)	0.771	0.784	0.766	0.767	0.793	0.779	0.701	0.750	0.731
SDPED_7 (Ours)	0.812	0.828	0.792	0.807	0.830	0.791	0.757	0.798	0.748
Improve	+5.3%	+5.2%	+3.4%	+4.5%	+3.4%	+1.5%	+5.7%	+4.7%	+2.3%
The results of the SDPED model with lengths 5 and 3 are listed below									
SDPED_5 (Ours)	0.811	0.824	0.795	0.806	0.827	0.796	0.756	0.793	0.744
SDPED_3 (Ours)	0.807	0.822	0.786	0.803	0.825	0.798	0.753	0.791	0.751

B. How big SDPED is?

Also note that our model employs the least number of coefficients among all compared models, as shown in Table VI. The size of our model is smaller than half of the previous ones, which could be surprising since it obtains comparable or better results. Such a situation demonstrates that the architecture of SDPED models could be more effective while a large number of coefficients in previous models might be wasted.

C. Do it effective in varied ED datasets?

On the other hand, our model could be more versatile compared with previous ones. As pointed out in [41], previous models obtained better scores on some datasets usually with the sacrifice on the scores on others. For example, the

experiments in the above section show that HED and RCF can outperform others on BRIND but are outperformed by others on UDED and BIPED2, and BDCN could perform best on UDED but not on other datasets, while Dexi and RIND provide best results on MDBD and BIPED2 but not on the other two. However, our model could obtain the best results on all the three benchmarks on most datasets, namely BRIND, UDED, and MDBD, while significantly outperforming previous models on AP with similar scores on other benchmarks on BIPED2. Therefore, our model could be more flexible on multiple datasets.

D. Limitation and Future works

Despite the effectiveness of SDPED models with fewer coefficients, their inference speed and GPU consumption might

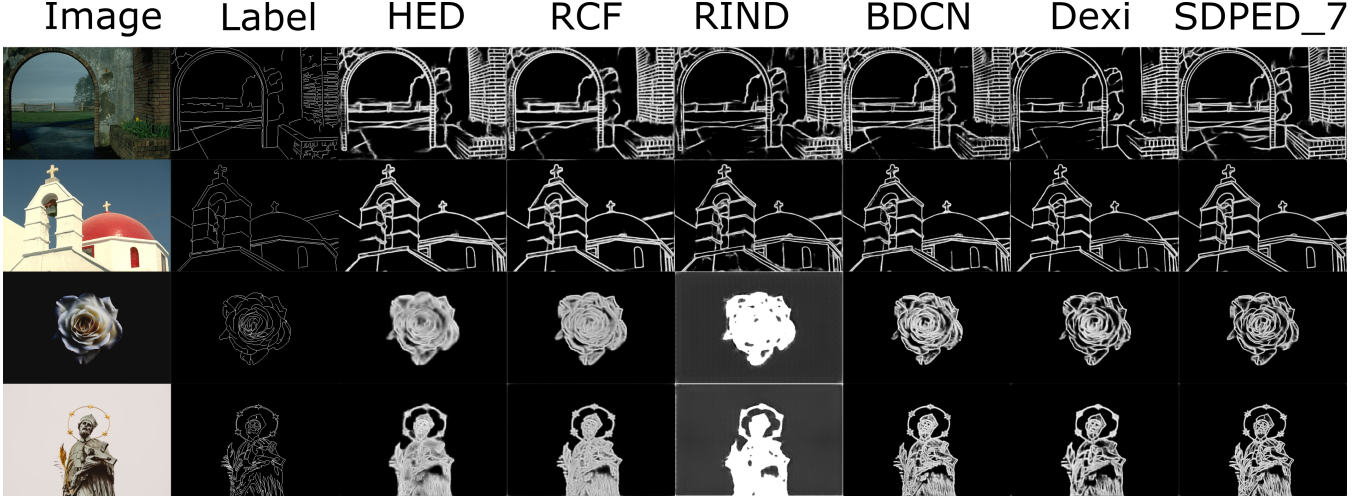


Fig. 6 Some predictions on BRIND and UDED, all are of partition P_1 and are displayed without NMS. Results demonstrate that our model can provide more comfortable predictions.

TABLE III

Results on MDBD with error toleration 0.001/0.003 (1.5 pixel / 4.4 pixels in horizontal and vertical), where the best results are marked as **blue**, while the second best ones are marked as **red**. The performance of all models is not satisfactory over the strictest standard (about 1.5-pixel error toleration). This might caused by the annotation quality. Therefore, an evaluation on a more relaxed standard (about 4.4 pixels error toleration) is also provided. In all the three experiments, all the three benchmarks, and all the two standards, our model obtains the best results. The improvements compared with the second-best ones are listed at the bottom. On average, the score of our model improves about 4.8%/2.5% on ODS, 4.8%/2.9% on OIS, and 22.5%/14.7% on AP, regarding error toleration 0.001/0.003, respectively. Note that the instability of RIND also occurs (please refer to P_1).

Partitions	MDBD- P_1 -60-40-E100			MDBD- P_2 -80-20-E100			MDBD- P_3 -80-20-E100		
Benchmarks	ODS	OIS	AP	ODS	OIS	AP	ODS	OIS	AP
HED	0.302/0.565	0.304/0.570	0.122/0.425	0.289/0.550	0.291/0.554	0.114/0.396	0.261/0.515	0.264/0.520	0.094/0.356
RCF	0.276/0.538	0.277/0.540	0.096/0.356	0.264/0.525	0.266/0.527	0.089/0.339	0.245/0.492	0.246/0.495	0.079/0.307
RIND	0.243/0.455	0.244/0.460	0.035/0.091	0.287/0.555	0.290/0.564	0.118/0.438	0.285/0.531	0.292/0.550	0.125/0.445
BDCN	0.277/0.542	0.278/0.545	0.104/0.377	0.270/0.533	0.273/0.536	0.097/0.362	0.255/0.514	0.257/0.515	0.088/0.339
Dexi	0.305/0.571	0.307/0.576	0.126/0.433	0.294/0.558	0.297/0.563	0.116/0.407	0.271/0.521	0.274/0.529	0.102/0.374
SDPED_7	0.327/0.590	0.330/0.599	0.165/0.531	0.309/0.569	0.312/0.579	0.148/0.501	0.291/0.543	0.297/0.561	0.139/0.477
Improve (%)	+7.2/+3.3	+7.5/+4.0	+31.0/+22.6	+5.1/+2.0	+5.1/+2.7	+25.4/+14.4	+2.1/+2.3	+1.7/+2.0	+11.2/+7.2

TABLE IV

Results on BIPED2 with error toleration 0.001 (1 pixel on diagonal), where the best results are marked as **blue**, while the second best ones are marked as **red**. The improvements of SDPED_7 compared with the best scores previously (on each partition and benchmark, no matter whether it is obtained by the same previous model or not) are listed at the bottom, while the average results of the three partitions are provided in the rightest columns. In summary, our model obtains comparable results to the previous ones in ODS and OIS (different less than 0.3% on average or less than 0.6% for single terms, no matter SDPED_7 or the previous ones obtain the best scores), while it significantly outperforms previous ones on AP (improves about 11.8% on average or at least 10.9% for single terms).

Partitions	BIPED2- P_1 -125-125-E75			BIPED2- P_2 -175-75-E75			BIPED2- P_3 -200-50-E75			Average		
Benchmarks	ODS	OIS	AP	ODS	OIS	AP	ODS	OIS	AP	ODS	OIS	AP
HED (2015)	0.640	0.643	0.493	0.645	0.648	0.496	0.640	0.644	0.494	0.642	0.645	0.494
RCF (2017)	0.641	0.644	0.509	0.644	0.647	0.510	0.640	0.644	0.497	0.642	0.645	0.505
RIND (2021)	0.673	0.674	0.479	0.688	0.691	0.468	0.677	0.681	0.341	0.679	0.682	0.429
BDCN (2022)	0.654	0.657	0.519	0.667	0.670	0.530	0.655	0.659	0.512	0.659	0.662	0.520
Dexi (2023)	0.674	0.675	0.530	0.683	0.685	0.544	0.677	0.679	0.530	0.678	0.680	0.535
SDPED_7 (Ours)	0.675	0.678	0.599	0.684	0.687	0.608	0.673	0.680	0.588	0.677	0.682	0.598
Improve	+0.1%	+0.4%	+13.0%	-0.6%	-0.6%	+11.8%	-0.6%	-0.1%	+10.9%	-0.3%	0.0%	+11.8%

TABLE V

The ablation result on BRIND and UDED, where *No skipping* represents that all skipping connections, namely the dashed lines (not including the residue ones) in SDB are deleted, *Single fuse* represents that only employs a single 1×1 convention layer as the final fusing block, and *No skipping with single fuse* represents that both all skipping connections are deleted and only employs a single 1×1 convention layer as the final fusing block. The best results are **bold**. The results demonstrate the validity of the structures.

Partitions	BRIND- P_1			UED- P_2			BIPED2- P_3		
Benchmark	ODS	OIS	AP	ODS	OIS	AP	ODS	OIS	AP
SDPED_7	0.660	0.672	0.613	0.807	0.830	0.791	0.677	0.682	0.598
SDPED_7 (No skipping)	0.654	0.664	0.589	0.776	0.803	0.772	0.670	0.676	0.577
SDPED_7 (Single fuse)	0.657	0.669	0.609	0.798	0.820	0.786	0.664	0.669	0.568
SDPED_7 (No skipping with single fuse)	0.649	0.660	0.581	0.786	0.812	0.751	0.666	0.670	0.565

need improvement. Since SDPED models are implemented on the full image resolution, the memory cost could be high and the inference speed might be lower than previous models. In this paper, we mainly focus on improving the performance of ED models over a high-standard benchmark but pay less attention to accelerating them. But in practice, it would be a trade-off between accuracy and consumption. The acceleration schemes and the reduction of the memory are left to the future works.

On the other hand, obtaining noiseless data for ED tasks could be a long-standing problem since edges do not have a formal definition¹³. Therefore, datasets for ED tasks are highly dependent on human labels, which are unavoidable noise. However, most problems in the model prediction might be traced back to data, which was also indicated in the experiments in Section IV, where most models perform better on UDED dataset with the highest quality even if the dataset contains the least number of training images. Although Section III B provides the first trick to obtain noiseless data, it is worth investigating further how to obtain more datasets with less noise.

TABLE VI

The sizes of the employed models, where the best are bold. Our model SDPED_7 has the least coefficients, only about 38.9% compared with the second smallest one (HED), while as has been shown, our model significantly outperforms HED in every experiment. For more details, the size of our model is about 38.9% of RCF, 9.6% of RIND, 35.1% of BDCN, and 16.3% of Dexi.

	Size (kB)	Num. of Coe. ($\times 10^6$)
HED (2015)	57499	14.716171
RCF (2017)	57850	14.803781
RIND (2021)	232593	59.388526
BDCN (2022)	63749	16.302120
Dexi (2023)	137775	35.215245
SDPED_7 (Ours)	22470	5.728638

VI. CONCLUSION

In this paper, we have presented novel precise ED models (SDPED) and provided a modification on data augmentation to improve the performance of models on noiseless data. Our

model obtains SOTA results, especially on improving the AP, over multiple datasets and different partitions, which demonstrates that it could be more precise and flexible than previous ones. Furthermore, the number of coefficients employed in our model is less than half of the previous SOTA models, which illustrates that its structure could be more effective and efficient. Finally, the modification of data augmentation provides the first method to employ noiseless data in training ED models, which could be widely employed in the future.

VII. BIBLIOGRAPHY

REFERENCES

- [1] C. H. Zhan, X. H. Duan, S. Y. Xu, Z. Song, and M. Luo. An improved moving object detection algorithm based on frame difference and edge detection. In *Fourth international conference on image and graphics (ICIG 2007)*, pages 519–523. IEEE, 2007.
- [2] R. Muthukrishnan and M. Radha. Edge detection techniques for image segmentation. *International Journal of Computer Science & Information Technology*, 3(6):259, 2011.
- [3] J. Kittler. On the accuracy of the sobel edge detector. *Image and Vision Computing*, 1(1):37–42, 1983.
- [4] J. Canny. A computational approach to edge detection. *IEEE Transactions on pattern analysis and machine intelligence*, PAMI-8(6):679–698, 1986.
- [5] S. Konishi, A. L. Yuille, J. M. Coughlan, and S. C. Zhu. Statistical edge detection: learning and evaluating edge cues. *IEEE Transactions on Pattern Analysis and Machine Intelligence*, 25(1):57–74, 2003.
- [6] P. Arbeláez, M. Maire, C. Fowlkes, and J. Malik. Contour detection and hierarchical image segmentation. *IEEE Transactions on Pattern Analysis and Machine Intelligence*, 33(5):898–916, 2011.
- [7] D.R. Martin, C.C. Fowlkes, and J. Malik. Learning to detect natural image boundaries using local brightness, color, and texture cues. *IEEE Transactions on Pattern Analysis and Machine Intelligence*, 26(5):530–549, 2004.
- [8] P. Dollar, Z. W. Tu, and S. Belongie. Supervised learning of edges and object boundaries. In *2006 IEEE Computer Society Conference on Computer Vision and Pattern Recognition (CVPR'06)*, volume 2, pages 1964–1971, 2006.

¹³In another view, if edges can be defined formally, traditional algorithms could have solved ED problems.

- [9] X. F. Ren. Multi-scale improves boundary detection in natural images. In *Computer Vision—ECCV 2008: 10th European Conference on Computer Vision, Marseille, France, October 12–18, 2008, Proceedings, Part III 10*, pages 533–545. Springer, 2008.
- [10] J. J. Lim, C. L. Zitnick, and P. Dollár. Sketch tokens: A learned mid-level representation for contour and object detection. In *Proceedings of the IEEE conference on computer vision and pattern recognition*, pages 3158–3165, 2013.
- [11] Y. Ganin and V. Lempitsky. n^4 -fields: neural network nearest neighbor fields for image transforms. In *Asian conference on computer vision*, pages 536–551. Springer, 2014.
- [12] P. Dollár and C. L. Zitnick. Fast edge detection using structured forests. *IEEE Transactions on Pattern Analysis and Machine Intelligence*, 37(8):1558–1570, 2015.
- [13] G. Bertasius, J. B. Shi, and L. Torresani. Deepedge: A multi-scale bifurcated deep network for top-down contour detection. In *Proceedings of the IEEE conference on computer vision and pattern recognition*, pages 4380–4389, 2015.
- [14] W. Shen, X. G. Wang, Y. Wang, X. Bai, and Z. J. Zhang. Deepcontour: A deep convolutional feature learned by positive-sharing loss for contour detection. In *Proceedings of the IEEE conference on computer vision and pattern recognition*, pages 3982–3991, 2015.
- [15] S. N. Xie and Z. W. Tu. Holistically-nested edge detection. In *Proceedings of the IEEE international conference on computer vision*, pages 1395–1403, 2015.
- [16] Y. Liu, M. M. Cheng, X. W. Hu, K. Wang, and X. Bai. Richer convolutional features for edge detection. In *Proceedings of the IEEE conference on computer vision and pattern recognition*, pages 3000–3009, 2017.
- [17] J. Z. He, S. L. Zhang, M. Yang, Y. H. Shan, and T. J. Huang. Bi-directional cascade network for perceptual edge detection. In *Proceedings of the IEEE/CVF conference on computer vision and pattern recognition*, pages 3828–3837, 2019.
- [18] M. Le and S. Kayal. Revisiting edge detection in convolutional neural networks. In *2021 International Joint Conference on Neural Networks (IJCNN)*, pages 1–9. IEEE, 2021.
- [19] J. K. Wibisono and H. M. Hang. Fined: Fast inference network for edge detection. In *2021 IEEE International Conference on Multimedia and Expo (ICME)*, pages 1–6. IEEE, 2021.
- [20] Z. Su, W. Z. Liu, Z. T. Yu, D. W. Hu, Q. Liao, Q. Tian, M. Pietikäinen, and L. Liu. Pixel difference networks for efficient edge detection. In *Proceedings of the IEEE/CVF international conference on computer vision*, pages 5117–5127, 2021.
- [21] L. X. Huan, N. Xue, X. W. Zheng, W. He, J. Y. Gong, and G. S. Xia. Unmixing convolutional features for crisp edge detection. *IEEE Trans. Pattern Anal. Mach. Intell.*, 44(10 Part 1):6602–6609, oct 2022.
- [22] M. Y. Pu, Y. P. Huang, Y. M. Liu, Q. J. Guan, and H. B. Ling. Edter: Edge detection with transformer. In *Proceedings of the IEEE/CVF conference on computer vision and pattern recognition*, pages 1402–1412, 2022.
- [23] X. Soria, A. Sappa, P. Humanante, and A. Akbarinia. Dense extreme inception network for edge detection. *Pattern Recognition*, 139:109461, 2023.
- [24] M. Pu, Y. Huang, Q. Guan, and H. Ling. Rindnet: Edge detection for discontinuity in reflectance, illumination, normal and depth. In *2021 IEEE/CVF International Conference on Computer Vision (ICCV)*, pages 6859–6868. IEEE Computer Society, oct 2021.
- [25] J. Z. He, S. L. Zhang, M. Yang, Y. H. Shan, and T. J. Huang. Bdcn: Bi-directional cascade network for perceptual edge detection. *IEEE Transactions on Pattern Analysis and Machine Intelligence*, 44(1):100–113, 2022.
- [26] X. Soria, Y. Li, M. Rouhani, and A. D. Sappa. Tiny and efficient model for the edge detection generalization. In *2023 IEEE/CVF International Conference on Computer Vision Workshops (ICCVW)*, pages 1356–1365. IEEE Computer Society, oct 2023.
- [27] X. Soria, E. Riba, and A. Sappa. Dense extreme inception network: Towards a robust cnn model for edge detection. In *2020 IEEE Winter Conference on Applications of Computer Vision (WACV)*, pages 1912–1921. IEEE Computer Society, mar 2020.
- [28] D. A. Mély, J. k. Kim, M. McGill, Y. L. Guo, and T. Serre. A systematic comparison between visual cues for boundary detection. *Vision Research*, 120:93–107, 2016. Vision and the Statistics of the Natural Environment.
- [29] X. T. Wang, L. B. Xie, C. Dong, and Y. Shan. Real-esrgan: Training real-world blind super-resolution with pure synthetic data. In *Proceedings of the IEEE/CVF international conference on computer vision*, pages 1905–1914, 2021.
- [30] D. Martin, C. Fowlkes, D. Tal, and J. Malik. A database of human segmented natural images and its application to evaluating segmentation algorithms and measuring ecological statistics. In *Proc. 8th Int’l Conf. Computer Vision*, volume 2, pages 416–423, July 2001.
- [31] N. N. Silberman, D. Hoiem, P. P. Kohli, and R. Fergus. Indoor segmentation and support inference from rgb-d images. In *European Conference on Computer Vision*, 2012.
- [32] M. Everingham, L. Van Gool, C. K. I. Williams, J. Winn, and A. Zisserman. The pascal visual object classes (voc) challenge. *International Journal of Computer Vision*, 88(2):303–338, jun 2010.
- [33] T. Y. Lin, M. Maire, S. Belongie, L. Bourdev, R. Girshick, J. Hays, P. Perona, D. Ramanan, C. L. Zitnick, and P. Dollár. Microsoft coco: Common objects in context. In *Computer Vision – ECCV 2014*, pages 740–755. Springer International Publishing, 2014.
- [34] B. L. Zhou, H. Zhao, X. Puig, S. Fidler, A. Barriuso, and A. Torralba. Scene parsing through ade20k dataset. In *2017 IEEE Conference on Computer Vision and Pattern Recognition (CVPR)*, pages 5122–5130, 2017.
- [35] M. Cordts, M. Omran, S. Ramos, T. Rehfeld, M. Enzweiler, R. Benenson, U. Franke, S. Roth, and B. Schiele.

The cityscapes dataset for semantic urban scene understanding. In *Proceedings of the IEEE Conference on Computer Vision and Pattern Recognition (CVPR)*, June 2016.

- [36] Y. B. Fu and X. J. Guo. Practical edge detection via robust collaborative learning. In *Proceedings of the 31st ACM International Conference on Multimedia*, MM '23, page 2526–2534. Association for Computing Machinery, 2023.
- [37] C. Wang, D. Dai, S. Xia, Y. Liu, and G. Wang. One-stage deep edge detection based on dense-scale feature fusion and pixel-level imbalance learning. *IEEE Transactions on Artificial Intelligence*, 5(01):70–79, jan 2024.
- [38] Y. P. Wang, X. Zhao, and K. Q. Huang. Deep crisp boundaries. In *2017 IEEE Conference on Computer Vision and Pattern Recognition (CVPR)*, pages 1724–1732, 2017.
- [39] R. X. Deng, C. H. Shen, S. J. Liu, H. B. Wang, and X. R. Liu. Learning to predict crisp boundaries. In *Computer Vision – ECCV 2018: 15th European Conference, Munich, Germany, September 8–14, 2018, Proceedings, Part VI*, page 570–586. Springer-Verlag, 2018.
- [40] X. T. Wang, K. Yu, S. X. Wu, J. J. Gu, Y. H. Liu, C. Dong, Y. Qiao, and C. C. Loy. Esrgan: Enhanced super-resolution generative adversarial networks. In *Computer Vision – ECCV 2018 Workshops*, pages 63–79, 2019.
- [41] M. Mubashar, N. Khan, A. R. Sajid, M. H. Javed, and N. U. Hassan. Have we solved edge detection? a review of state-of-the-art datasets and dnn based techniques. *IEEE Access*, 10:70541–70552, 2022.